



Electrostatic charging of the sunlit hemisphere of the Moon under different plasma conditions

R. Kureshi¹ · K.R. Tripathi² · S.K. Mishra³ 

Received: 25 November 2019 / Accepted: 3 February 2020 / Published online: 6 February 2020
© Springer Nature B.V. 2020

Abstract Accounting for the continuous interaction of the solar radiation, the development of electrostatic charge on the sunlit lunar regolith under extreme plasma conditions has been investigated—the ambient plasma around Moon corresponds to the plasma parameters associated with the solar wind, wake region, SEP events, and terrestrial magnetosphere. The photoemission of electrons from the lunar surface corresponding to the solar radiation spectrum, electron energy-dependent secondary electron emission and simultaneous collection of the ambient non-Maxwellian plasma electrons/ions have been considered the dominant charging mechanisms. The lunar surface potential has been derived using the dynamical balance of the photoemission and plasma accretion currents over its surface—the potential dependence of the charging currents has consistently been accounted for. In results, the lunar surface potential dependence on the plasma, surface, and radiation parameters have been parametrically derived. For the high temperature plasma composition, the sunlit locations over the lunar surface are predicted to acquire a negative potential. The outcome infers that depending on topography and location along with realistic plasma/surface parameters, the lunar surface may hold significant contrast in charging, and it may differ by the orders of magnitude. Such disparity in the surface charging may act as a source of the transport of charged dust and local atmospheric charge (ions/electrons) over the lunar regolith.

Keywords Moon · Sunlit hemisphere · Photoemission · Differential charging · Charge transport

1 Introduction

The Moon orbiting Earth, depending on its phases, encounters with solar radiation and local plasma—in response to these currents, the exposed lunar surface acquires a finite charge, and subsequently leads to a plasma environment over its surface (Nitter et al. 1998; Stubbs et al. 2007a; Sternovsky et al. 2008; Poppe and Horanyi 2010). The ambient plasma (Halekas et al. 2008, 2009a) usually corresponds to the solar wind, terrestrial magnetosphere and solar energetic particles (SEPs), and vary in terms of number density, energy distribution, and mean temperature (Halekas et al. 2002). For instance, Lunar Prospector (LP) Electron Reflectometer (ER) observations suggest that the sunlit hemisphere of Moon encounters low temperature flowing plasma, while the wake region is characterised by high-temperature plasma with relatively lower electron density (Halekas et al. 2008). In exotic conditions, transient solar events such as SEP events can contribute very energetic plasma currents to the surface for brief periods (Halekas et al. 2009a). The terrestrial magnetosphere comprises of rarefied plasma density ($\sim 0.1 \text{ cm}^{-3}$), but differ in terms of particle energy (Halekas et al. 2008)—magnetotail lobes corresponds to $< 100 \text{ eV}$ electrons, while the plasma sheet and magnetosheath possess relatively high energy electrons ($\sim 0.1\text{--}2 \text{ keV}$). Such variation in plasma fluxes significantly influences the lunar surface charging. In a typical solar wind wake case, the lunar surface is observed to acquire $\sim 100 \text{ V}$ negative potential (Halekas et al. 2002, 2008), while in a terrestrial plasma sheet, the lunar surface is measured to gain $\sim -500 \text{ V}$, despite the continuous solar illumination (Poppe et al. 2011).

✉ S.K. Mishra
nishfeb@gmail.com; sanjaym@prl.res.in

¹ Cummins Engineering College of Women, Pune 411052, India

² Space Physics Laboratory, Thiruvananthapuram 695021, India

³ Physical Research Laboratory, Ahmedabad 380009, India

The sunlit hemisphere induces the photoemission of electrons from the lunar regolith and is significant in determining the surface charging. Based on SIDE (Suprathermal Ion Detector Experiment) solar wind data, Goldstein (1974) calculated the surface potential in the range (−3 V to 5 V) on Apollo 12 and Apollo 15 sites. The charging of the night side of the Moon is dominated by the plasma constituents associated with aforesaid plasma populations and may get a charge to very high negative potential (Stubbs et al. 2007a).

Apart from the plasma population, the difference in lunar regolith material composition may also lead to variation in surface potential, particularly the sunlit surface where photoemission significantly contributes to the charging process. Noted, most of the earlier analysis for the photoemission charging generally takes account of a constant photoemission current (Stubbs et al. 2007b, 2014; Poppe et al. 2012; Piquette and Horanyi 2017)—these analyses ignore the surface potential dependence of the photoemission current. The topography of the lunar surface in the form of craters and boulders, is another interesting site, might lead to a complex electrostatic potential and fields, locally (Poppe et al. 2012)—it includes the phenomena of mini wakes in the rear part of small obstacles facing the solar wind and supercharging around sunlit-shadowed regions. Another concern is the variation of the lunar surface temperature with latitude, which is a significant parameter defining the electron population available for the photoemission within the surface lattice (Fowler 1955). According to the Lunar Reconnaissance Orbiter (LRO) based Diviner Lunar Radiometer Experiment (Williams et al. 2017), the temperature of the lunar regolith is observed to vary between (400 K–150 K) from the subsolar point to terminator region. In this work, we revisit the analysis of the lunar regolith charging by including few missing aspects and calculate the electrical potential on the lunar surface in various plasma conditions.

As a novel feature, in deriving the photoemission flux from the sunlit lunar regolith, we take account of Fowler's theory of the photoelectron emission by including Fermi Dirac (FD) velocity (or energy) distribution of electrons within regolith lattice and full solar spectrum (Bauer 1973; Misra and Mishra 2013). The consideration of FD statistics (Fowler 1955) is physically more consistent with the lunar surface operating at low-temperature regime (~ 150 K–400 K)—this is a significant distinction from earlier studies (Halekas et al. 2008; Stubbs et al. 2007b; Whipple 1981), where the oversimplified Maxwellian distribution has been used. In deriving the surface potential, the latitude dependence of the regolith temperature is also taken into account; this is a significant parameter in determining the electron population density available for emission within lattice (Fowler 1955). The significance of Fermionic energy distribution of the lattice electrons on the photoelectron sheath (i.e., local plasma atmosphere) has been

highlighted in Sodha and Mishra (2014) and Mishra and Bhardwaj (2019). The plasma populations around Moon relevant to dark/sunlit phases have been taken from Table-1 of Halekas et al. (2008), where LP-ER based electron features in different physical conditions like solar wind, wake, terrestrial magnetospheric tail lobe, and plasma sheets, and SEP events, have been summarised. We use the collection flux associated with these plasma populations in deriving the surface potential of lunar regolith in such circumstances. In addition, the inclusion of Kappa distribution of electrons in the plasma population around Moon is another difference from the earlier analysis. Considering the high energy plasma environment around the Moon, we also include the phenomenon of secondary electron emission (Whipple 1981; Meyer-Vernet 1982) as the source of electron generation from the lunar regolith. The electron energy dependence of the secondary electron emission (SEE) yield corresponding to the adequate plasma energy distribution has consistently been accounted for deriving the effective SEE current. The charging of the lunar surface is considered as the dynamic balance of incoming (plasma electron/ion) and outgoing (emitted electron) currents. Based on the formulation, we parametrically analyse and illustrate the charging of the lunar surface under the influence of a wide variety of plasma environments in dark/shadow and sunlit hemispheres. The essence of the work is to bring out the physics insight of the electrostatic charging of the lunar surface under extreme plasma conditions and the coexisting phenomena of photoemission and SEE.

2 Determination of surface potential

Depending on the location in orbit, the Moon goes through various plasma environments and solar illumination—the charging of the lunar surface occurs primarily through the collection of plasma electrons/ions, secondary electron emission (SEE) and photoemission. The transient evolution of the lunar surface potential may be expressed as (Sodha et al. 2009)

$$\frac{dv_s}{dt} = c_1 \left[f_{ph} + \left(\sum_j \eta_{i,j} f_{ic,j} - \sum_j \eta_{e,j} f_{ec,j} \right) + \sum_j \delta_j \eta_{e,j} f_{ec,j} \right], \quad (1)$$

where $v_s = -eV_s/kT$, $V_s = 4\sigma(\sinh^{-1} 1)$ is the electric field potential on the planar surface of unit length (Ciftja 2011) with the surface charge density σ , $c_1 = (-4e^2/kT)(\sinh^{-1} 1)$, f_{ph} represents the photoemission current, while f_{ec} and f_{ic} correspond to the effective collection current associated with the plasma electrons and ions,

respectively, η_e (η_i) refers to the sticking coefficient of the electron (ions) to the accreting surface, δ is the Secondary electron emission (SEE) yield of the lunar surface material, the summation includes all sorts of the plasma environment (j 's), applicable to the physical situation under consideration. The expressions of relevant processes are given later in the text.

Equation (1) describes the temporal evolution of the charge on the location of interest. Its magnitude depends on the solar irradiation and local plasma environment, like solar wind, SEP, wake, and terrestrial magnetosphere. The first term in the square bracket represents the rate of photoelectron generation per unit area due to the solar illumination. The solar illumination over the Moon surface is unidirectional, and the magnitude of the photon flux over the sunlit hemisphere depends on its latitude. Accounting large curvature of the Moon, for all practical realisations, an elementary region of interest may be considered as of planar geometry—this is used later in the analysis. The second term in the small bracket in Eq. (1) corresponds to the rate of net charge collection over a unit area over the lunar surface, associated with the ambient plasma electrons–ions composition. The last term in the square bracket refers to the secondary electron emission flux due to the impact of high energy primary electrons over the lunar regolith. Next, we briefly describe the electron and ion currents related to the aforesaid charging processes.

3 Photoemission flux from sunlit regolith

Following Bauer (1973), the solar radiation may be considered to comprise of the continuous white light spectrum (> 190 nm) in addition to dominant Extreme Ultraviolet (EUV) Lyman- α (121.57 nm) spike. Practically, the continuous solar radiation may be expressed as a black body object radiating at 5800 K. Both, viz., continuous and Lyman- α radiations are considered inducing photoelectrons from the sunlit hemisphere of the Moon. Intuitively, the continuous spectrum may be significant for the low work function regolith material, while Lyman- α contribution dominates in determining the photoemission current. The net solar photon flux incident on the lunar surface at θ latitude may be written as

$$\begin{aligned} \Lambda_{inc} &= \left[\int_{E_{v0}}^{E_{vm}} d\Lambda_{cr} + \Lambda_{L\alpha} \right] \cos\theta \\ &= \left[\left(\frac{r_s^2}{r_d^2} \right) \int_{E_{v0}}^{E_{vm}} f_v dE_v + \Lambda_{L\alpha} \right] \cos\theta, \end{aligned} \tag{2}$$

where $f_v = (2\pi/c^2)(e/300h)^3 E_v^2 [\exp(E_v/kT_s) - 1]^{-1}$ refers to Planck's distribution function, r_s ($= 6.96 \times 10^{10}$ cm) and T_s ($= 5800$ K) are the radius and temperature of the radiating body, i.e., the Sun, respectively, r_d ($= 1.49 \times$

10^{13} cm) is the mean distance between the Sun and the Moon, Λ_{cr} and $\Lambda_{L\alpha}$ ($= 3 \times 10^{11}$ cm $^{-2}$ s $^{-1}$), respectively, are the photon flux associated with continuous and EUV Lyman- α spike in the solar spectrum (Bauer 1973), the integral limits E_{v0} ($= \phi + V$) and E_{vm} correspond to the useful solar spectrum, ϕ and V are the work function and potential of the regolith surface, and h , k , and e are the Planck's constant, Boltzmann's constant and electronic charge; here E_v is expressed in eV. Here, the latitude (θ) of the desired location on the lunar regolith is measured from the subsolar point towards limb (along latitudinal direction)—for clarity of this convention, we refer Fig. 1 of Mishra and Bhardwaj (2019).

Considering Fowler's approach of the photoelectron emission (Fowler 1955) and Fermi Dirac energy statistics of the lattice electrons (Seitz 1940), the momentum distribution of the emitting photoelectrons flux, normal to the surface having potential V_s , can be expressed as (Mishra and Bhardwaj 2019)

$$\begin{aligned} dn_{ph}(v_s) &= \cos\theta \left[\int_{E_{v0}}^{E_{vm}} (\chi_v/\Phi_v) \ln[1 + \exp[-(\varepsilon_x - \zeta_v)]] d\varepsilon_x d\Lambda_{cr} \right. \\ &\quad \left. + (\chi_{L\alpha}/\Phi_{L\alpha}) \Lambda_{L\alpha} \ln[1 + \exp[-(\varepsilon_x - \zeta_{L\alpha})]] d\varepsilon_x \right], \end{aligned} \tag{3}$$

where χ is the photoefficiency of surface material, $\zeta = (\varepsilon_i - \varphi)$, $\varphi = e\phi/kT$, $\varepsilon_i = E_i/kT$, $\varepsilon_{vm,0} = E_{vm,0}/kT$, $v_s = -(eV_s/kT)$, ε_x ($= E_x/kT$) refers the dimensionless energy of the electrons normal to the surface, $\Phi(\zeta) = \int_0^{\exp\zeta} \Omega^{-1} \ln(1 + \Omega) d\Omega$, and the subscript j refers to v (continuous spectrum) and $L\alpha$ (Lyman- α radiation).

The rate of photoemission from the lunar surface may be obtained by integrating Eq. (3) within appropriate boundaries over the normal energy—the additional potential barrier comes from the surface charge. If the surface is at finite positive potential, the limits of integration correspond to $\varepsilon_x \in (-v_s, \infty)$ while for the negatively charged surfaces this limit refers to $\varepsilon_x \in (0, \infty)$. Thus, the net photoemission rate may algebraically be expressed as,

$$n_{ph}(v_s) = \int_{-v_s,0}^{\infty} dn_{ph}(v_s). \tag{4}$$

The positive potential barrier for the photoemission from the lunar surface apparently also describes and takes account of the effect of the photoelectron sheath (Sodha and Mishra 2014) in the electron emission/collection. Noted, that the photoelectron sheath formation is effectively the screening of positively charged lunar surface. Equation (4) infers that the photoemission current depends on the density population of electrons within the distribution, which is a significant function of the temperature of the emitting surface.

Based on LRO Diviner observations (Williams et al. 2017), the lunar regolith temperature varies from 400 K (subsolar) to 150 K (terminator) over the sunlit hemisphere. Accounting a linear dependence over the latitude, the regolith temperature may be expressed as $T_\theta = T_0[1 - (5/4\pi)\theta]$. With this, higher photoelectrons flux near the subsolar points is anticipated. The photoemission flux causes an electron cloud in the vicinity of the emitting surface. For a positively charged surface, the electrons leaving and returning to the lunar surface contribute to the photoelectron population. Using Eq. (3), the photoelectron population density just on the top of the emitting surface can be written by integrating the expression $dn_{pe}(v_s) = (m/2kT)^{1/2}\varepsilon_x^{-1/2}dn_{ph}(v_s)$, over appropriate limits; where m is the electronic mass. Following Draine (1978), the spectral dependence of the photoelectric efficiency is given by $\chi_v = \chi_o(1 - \phi/E_v)$, where χ_o is the optimum value of the photoelectric yield. Next, we define the rate of electron/ion collection over the surface.

4 Plasma collection over lunar regolith

The charging current associated with different plasma populations around lunar regolith depends on the energy distribution of the constituent particles (electrons/ions). In different physical scenarios around Moon, based on LP measurements, the energy distribution of the electrons accreting on the lunar regolith is characterised by a non-Maxwellian Kappa distribution (Halekas et al. 2008, 2009a); algebraically this may be expressed as

$$f_\kappa(v) = \beta(\pi\gamma v_T^2)^{-3/2} [1 + (v^2/\gamma v_T^2)]^{-(\kappa+1)} dv, \quad (5)$$

where v refers to the total particle velocity, $v_T = (2kT_p/m)^{1/2}$ corresponds to the thermal speed of the electrons, T_p is the thermal temperature, $\gamma = (\kappa - 3/2)$, $\beta = [\Gamma(\kappa + 1)/\Gamma(\kappa - 1/2)]$ and κ refers to the spectral index of distribution.

In comparison to the usual Maxwellian distribution, depending on κ , the Kappa statistics reflect a large density population in the high energy distribution tail. In LP measurements, the energy distribution $\kappa \geq 2$ is frequently observed. Under the influence of Debye shielding and Interplanetary Magnetic Field (IMF), the electrons and ions in solar wind plasma at 1 AU may exhibit Kappa distribution (Livadiotis et al. 2018)—this is also in concurrence with the plasma quasi-neutrality. Considering this physics insight, consistency with electron energy distribution and completeness in the analysis, we consider both the cases viz. non-Maxwellian Kappa distribution and Maxwellian nature of the ambient plasma ions. Based on Orbital Motion Limited (OML) approach, the accretion flux, i.e., the rate of collection per unit area per unit time, associated

with plasma electrons/ions over the lunar surface having potential V_s , may be expressed as (Mishra et al. 2013; Mishra and Misra 2014)

For $v_s \leq 0$:

$$f_{ec} = n_{es,j} \left(\frac{\gamma k T_{es,j}}{2\pi m} \right)^{1/2} \left(\frac{\Gamma(\kappa - 1)}{\Gamma(\kappa - 1/2)} \right) \times [1 - (\kappa - 1)(v_s/\gamma)(T/T_{es,j})], \quad (6a)$$

$$f_{ic} = n_{is,j} \left(\frac{\gamma k T_{is,j}}{2\pi m_i} \right)^{1/2} \left(\frac{\Gamma(\kappa - 1)}{\Gamma(\kappa - 1/2)} \right) \times [1 - (q_i v_s/\gamma)(T/T_{is,j})]^{1-\kappa}, \quad (6b)$$

For $v_s > 0$:

$$f_{ec} = n_{es,j} \left(\frac{\gamma k T_{es,j}}{2\pi m} \right)^{1/2} \left(\frac{\Gamma(\kappa - 1)}{\Gamma(\kappa - 1/2)} \right) \times [1 + (v_s/\gamma)(T/T_{es,j})]^{1-\kappa}, \quad (6c)$$

$$f_{ic} = n_{is,j} \left(\frac{\gamma k T_{is,j}}{2\pi m_i} \right)^{1/2} \left(\frac{\Gamma(\kappa - 1)}{\Gamma(\kappa - 1/2)} \right) \times [1 + (\kappa - 1)(q_i v_s/\gamma)(T/T_{is,j})], \quad (6d)$$

here q and m_i refer to the ion charge in electronic units and mass, respectively, n_{es} (T_{es}) and n_{is} (T_{is}) correspond to the number density (mean temperature) of the electrons and ions, respectively, the subscript j refers to j th kind of plasma population. In contrast, if the plasma is of Maxwellian in nature, the accretion current can be written as

For $v_s \leq 0$:

$$f_{ec,j} = (kT_{es,j}/2\pi m)^{1/2} n_{es,j} [1 - v_s(T/T_{es,j})], \quad (7a)$$

$$f_{ic,j} = (kT_{is,j}/2\pi m_i)^{1/2} n_{is,j} \exp[q_i v_s(T/T_{is,j})], \quad (7b)$$

For $v_s > 0$:

$$f_{ec,j} = (kT_{es,j}/2\pi m)^{1/2} n_{es,j} \exp[-v_s(T/T_{es,j})], \quad (7c)$$

$$f_{ic,j} = (kT_{is,j}/2\pi m_i)^{1/2} n_{is,j} [1 + q v_s(T/T_{is,j})]. \quad (7d)$$

The dependence of the collection current on the surface potential has been illustrated by Mishra et al. (Mishra et al. 2013) where the quantitative estimate of the accretion current and dust charging corresponding to Kappa distribution is shown to approach the Maxwellian statistics based results for a large value of the spectral index ($\kappa \rightarrow \infty$). We compare the two cases for the set of parameters consistent with the plasma around the Moon in terms of the lunar surface potential.

5 Secondary electron emission flux

The high energy electrons associated with the plasma population around Moon may lead to a return (positive) current in form of the secondary electrons (Whipple 1981; Meyer-Vernet 1982; Chow et al. 1993) from its surface. The phenomenon has been intensively investigated both in laboratory experiments (Pavlu et al. 2008; Mann et al. 2011) and in computer simulations (e.g., Richterova et al. 2012, 2016; Misra et al. 2013). We include this effect in our calculations and use the formulation of Chow et al. (1993) for describing the electron energy dependence of the SEE yield; the analytical form may be expressed as,

For $v_s \leq 0$:

$$\delta_j(T_{es,j}) = [1 - v_s(T/T_s)] \exp[v_s(T/T_s)] \times \int_{-v_s(T/T_s)}^{\infty} \varepsilon \delta_\varepsilon \exp(-\varepsilon) d\varepsilon, \quad (8a)$$

For $v_s > 0$:

$$\delta_j(T_{es,j}) = \int_0^{\infty} \varepsilon \delta_\varepsilon \exp(-\varepsilon) d\varepsilon, \quad (8b)$$

and

$$\delta_\varepsilon = 7.4 \delta_m (E/E_m) \exp[-2(E/E_m)^{1/2}], \quad (8c)$$

here Eq. (8c) corresponds to the Sternglass (1954) expression for the SEE yield, $\varepsilon = E/kT_{es,j}$, δ_m is the optimum value of the SEE yield peaking at primary electron energy E_m and T_s is the thermal energy of the emitted secondary electrons which usually follows a Maxwellian velocity distribution with a mean energy of ~ 1 –5 eV (e.g., Goertz 1989). In our calculations we use $T_s = 2.5$ eV (Sternglass 1954). An interesting feature is that the SEE yield depicts an optimum with respect to incident primary electron energy (T_{es})—the net SEE current also follows a similar trend.

In charging calculations, δ_m and E_m are the significant parameters determining the SEE flux from the lunar surface—for lunar regolith, δ_m may take optimum value ~ 3.5 at $E_m = 400$ eV (Horanyi et al. 1998; Nemecek et al. 2011). In order to explain the LP observations of negative lunar surface potential, Halekas et al. (2009b) argued a reduction of effective SEE yield of dust covered lunar surface in comparison to the smooth surfaces. This fact is supported by Pivi et al. (2008) where a sharp reduction optimum SEE yield ($\sim 50\%$) is predicted for the grooved surfaces. In another investigation by Anderegg et al. (1972), a significant reduction (approximately a factor of ~ 2.6) is measured for the lunar regolith sample. In a recent simulation work, Richterova et al. (2016) have shown that the SEE yield of

the surface covered by dust cluster by a factor of 1.5 with respect to the yield of a smooth surface. In reference to the lunar plasma environment during earth Magnetosphere crossing, Vaverka et al. (2016) accounted for the reduced SEE yield as a variant to explore the conditions under which and the areas where a levitation of the lifted dust grains could be observed. In view of these aforesaid studies, we consider a plausible range of $\delta_m \sim (0.1$ – $2.0)$ and $E_m = 400$ eV in our calculations. This additional SEE return current from the lunar surface aid photoemission flux and ion accretion current in neutralising the electron flux on the surface.

6 Computational approach and physical parameters

The temporal evolution and steady-state values of the surface potential at any given location over lunar regolith can be obtained by solving the charging equation (Eq. (1)), using the expressions for the plasma collection current (Eq. (6a)–(6d)) and (Eq. (7a)–(7d)) and photoemission flux (Eq. (4)), along with adequate plasma parameters. We use the numerical differential equation solver (NDSolve) of Mathematica software to solve the differential equation (Eq. (1)), where the initial condition is chosen as $V_s = 0$ at $t = 0$. With this, the surface potential has been parameterised as a function of the plasma density/temperature, spectral index κ , lunar latitude, photon flux, and regolith material (work function/photoefficiency).

As discussed earlier, the plasma features around Moon varies depending on its phase and location in its orbit. The LP-based measurements of electrons in the ambient plasma population in terms of (number density n_{es} , mean thermal temperature T_{es}) are as follows (Halekas et al. 2008): Terrestrial magnetosphere: Tail lobe (0.001 – 0.5 cm^{-3} , < 0.1 keV); Plasma sheet (0.01 – 1.0 cm^{-3} , 0.1 – 2 keV); Solar wind (0.5 – 10 cm^{-3} , 5 – 30 eV); Plasma wake (0.001 – 0.1 cm^{-3} , 50 – 150 eV); SEP event (0.001 – 0.1 cm^{-3} , 0.05 – 1 keV). The ambient plasma around the Moon may vary in terms of number density and temperature in exotic cases like solar flares and eruption events (Mann et al. 2004, 2011; Johansson 2009). In exotic conditions corresponding to extreme solar activities (Gosling et al. 1977; Pierrard et al. 2001), the solar wind plasma density is reported to reach ~ 100 cm^{-3} . We cover the entire range of the plasma properties in our computation, i.e., $n_{es} \sim (0.001$ – 100 $\text{cm}^{-3})$ and $T_{es} \sim (1$ eV– 2 keV). Following Draine and Salpeter (1979) and Weingartner and Draine (2001), $\eta_e = 1/2$ and $\eta_i = 1$ are taken as the sticking coefficient of electrons and ions, respectively. In order to address the effect of secondary electron emission, the electron plasma energy distribution has been consistently manifested with the electron energy dependent SEE yield (Eq. (8a)–(8c)). Considering the discussion in Sect. 5, we take a range of $\delta_m \sim (0.1$ – $2.0)$ and

$E_m = 400$ eV for calculations. For computations, the quasi-neutrality of the ambient plasma, i.e., $n_{es} \approx n_{is} \approx n_{so}$ along with $T_{es} \approx T_{is}$, is considered as the standard case. Additionally, we have also treated δ_m , (n_{es}/n_{is}) and (T_{es}/T_{is}) as a variant in our calculations.

In deriving the photoelectron flux from the lunar regolith, the incident solar photon flux is considered to include the continuous radiation ($\lambda > 190$ nm ~ 6.6 eV) from a black body object (i.e., the sun) radiating at $T_s = 5800$ K, and dominant EUV Lyman α radiation (121.57 nm ~ 10.3 eV). The photoelectric efficiency is a significant parameter determining the photoelectron flux from the lunar regolith. Kimura (2016) has derived and tabulated the photoefficiency of the fine particles and bulk material; in the spectral region of our interest ($> \phi$) for bulk silicate, it takes a value of the order of ~ 0.001 . We consider the optimum photoelectric efficiency $\chi_o = 0.001$ for our calculations. This choice refers to photoemission current $\sim 10 \mu\text{Am}^{-2}$ from an uncharged surface at subsolar point—this estimate is consistent with the earlier predicted photoemission current ($\sim 5 \mu\text{Am}^{-2}$) from the lunar regolith (Hinteregger et al. 1965; Stubbs et al. 2014); however, these values are slightly lower than estimates (10–80 μAm^{-2}) for the metallic and insulating materials at 1 AU (Whipple 1981; Zaslavsky 2015). It is noticed that the photoelectric yield of the fine particle and bulk yields varies significantly (Kimura 2016; Sickafoose et al. 2001); considering the dust rich lunar surface, we have also treated χ_o as a varying parameter in our numerical calculations. The surface temperature at the subsolar point (at $\theta = 0$) is taken as $T_0 = 400$ K, while a linear dependence is considered to calculate surface temperature T ($= T_\theta$) at any arbitrary latitude. Another significant parameter defining photoemission flux is the regolith work function. Following Grobman and Blank (1969), it may vary in the range $\phi \sim (4\text{--}6)$ V for the region across the subsolar point and limb. The effect of constituent parameters on the characteristic features of the lunar surface charging in terms of the electric potential has been parametrically investigated; in calculations, the work function (ϕ) and photoefficiency (χ_o) have been considered as varying parameters.

7 Numerical results and discussion

First, we discuss the charging of shaded or dark regions over lunar regolith which is not exposed to the solar radiation—this may correspond to the wake region (the dark hemisphere), shadowed portion of local topography in the form of highland, craters, and boulders, or artificial/man-made objects. In such locations, in the absence of photoemission (we refer it as dark region plasma) from the lunar regolith, the plasma population principally contributes to the surface charging on account of the constituent electron/ion collection. To begin with, we consider the case $\delta_m = 0$ (i.e., no

SEE), and the plasma electron and ion collections are dominant charging mechanisms. Due to the larger inertia of ions, the surface usually acquires a finite negative potential, of course, the magnitude and nature of the surface charge may vary depending on the plasma composition. In the steady-state ($d/dt \rightarrow 0$), the equation of surface charging (Eq. (1)), corresponding to a plasma population, can be expressed as

$$f_{ic} = f_{ec}. \quad (9)$$

Substituting the expressions for electron/ion collection flux corresponding to Kappa (Eq. (6a)–(6d)) and Maxwellian (Eq. (7a)–(7d)) distribution, Eq. (9) respectively reduces to

$$\tau^{1/2} \mu^{1/2} y z \exp(-x/\tau) = (1 + q_i x), \quad (10)$$

$$\begin{aligned} \tau^{1/2} \mu^{1/2} y z [1 + (x/\gamma\tau)]^{1-\kappa} \\ = [1 + q_i(\kappa - 1)(x/\gamma)], \end{aligned} \quad (11)$$

where $\tau = (T_{es}/T_{is})$, $y = (n_{es}/n_{is})$, $z = (\eta_e/\eta_i)$, $\mu = (m_i/m)$ and $x = (-eV_s/kT_{is})$.

Further, as another interesting case, if one considers a plasma with Maxwellian ions and Kappa distributed electrons, the flux balance can be written as,

$$\tau^{1/2} \mu^{1/2} y z [1 + (x/\gamma\tau)]^{1-\kappa} = (1 + q_i x). \quad (12)$$

Interestingly, the steady-state flux balance (Eq. (9)) reduces to a simpler form, where the lunar surface potential may be expressed as a function of dimensionless parameters τ , μ , and y . Physically, τ and y refer to the relative thermal energy and number density of the electrons, respectively, in the plasma distribution, while μ corresponds to ion mass. The dependence of parameter x , i.e., the lunar surface potential on the spectral index (κ) has been illustrated in Fig. 1a; the computations correspond to quasi-neutral electron-proton plasma ($y = 1$) for $\tau = 1$, and $z = (1/2, 1.0)$. The surface acquires higher potential in the case of plasma comprising of Kappa distribution than that of Maxwellian plasma. This may be attributed to the large population density of high energy electrons associated with Kappa distribution. In case when Maxwellian ions balance Kappa distributed electrons, the surface acquires a slightly higher negative potential (magenta curve, Eq. (11)); this may be understood in terms of reduced ion flux. The potential estimates (Eqs. (10)–(11)) for Kappa distribution approaches to Maxwellian based estimate (Eq. (10)) for large κ values. Smaller the surface potential for $z = 1/2$ may be understood in terms of reduction in electron density by half, and hence the reduction of electron collection current by a factor of $(1/z)$, i.e., 2—the reduced flux causes a smaller magnitude of the surface potential. The figure also suggests that in the steady-state, the dark/shadowed locations on the lunar surface may acquire

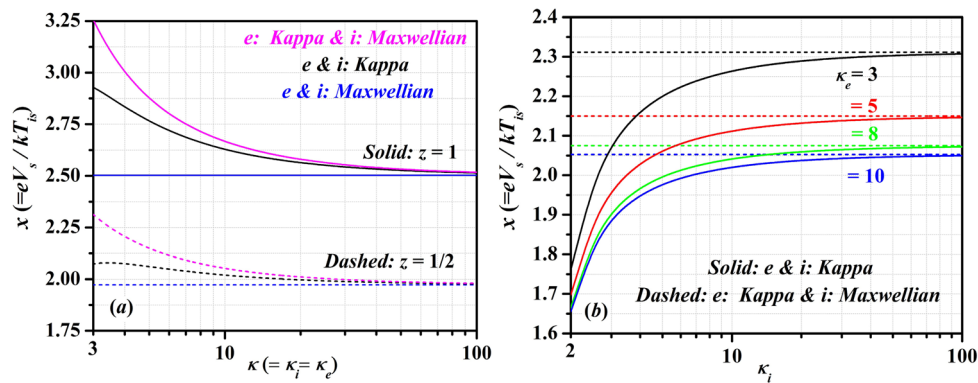
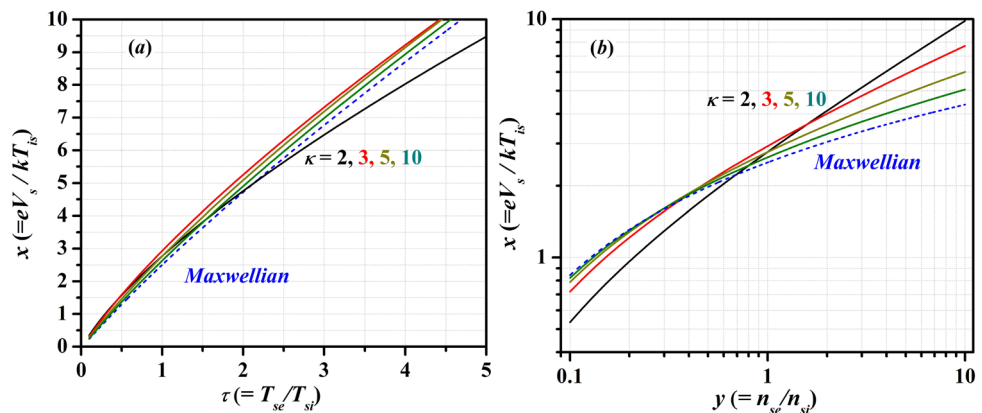


Fig. 1 Dependence of the parameter x on the spectral index κ in the absence of electron emission; the computations correspond to $y = 1$ and $\tau = 1$. **(a, left panel):** x as a function of κ ($\kappa_e = \kappa_i$); the solid and dashed lines refer to $z = 1$ and $z = 1/2$, respectively. The black and blue colour labels refer to Kappa and Maxwellian velocity distribution of the plasma electrons/ions, respectively, while the magenta colour

curve corresponds to Kappa distributed electrons and Maxwellian ions. **(b, right panel):** x as a function of κ_i for different values of κ_i for $z = 1/2$; the solid lines refer Kappa distribution of the plasma electrons/ions, while dashed lines correspond to Kappa distributed electrons and Maxwellian ions. The black, red, green and blue colour lines correspond to $\kappa_e = 3, 5, 8$ and 10 , respectively

Fig. 2 Dependence of the parameter x on the parameter τ **(a: left panel)** and y **(b: right panel)** in the absence of electron emission. The computations correspond to $y = 1, \tau = 1$ and $z = 1$. The colour labels black, red, grey and green in figures refer to the magnitude of the varying parameter $\kappa = 2, 3, 5$ and 10 , respectively. The blue colour dashed line corresponds to the Maxwellian velocity distribution of the plasma electrons/ions



negative potential nearly of the order of the plasma temperature. The calculations predict slightly higher (approximately ~ 1.16 – 1.3 times for $\kappa \sim 3.0$ and $z = 1$) lunar potential corresponding to Kappa distribution than that of Maxwellian plasma. For instance, for $T_{es} = T_{is} = 10$ V, the lunar surface holds a negative potential of ~ 25 V and $\sim (29.0$ – $32.5)$ V for ($\kappa \sim 3.0$ and $z = 1$) respectively, for Maxwellian and Kappa statistics. Figure 1b depicts the effect of ion distribution (for different values of κ_i) on the surface charging. It is observed that the lunar surface potential marginally differs from the Maxwellian ion distribution for the moderate values of κ_i (~ 5 – 10). The difference in the surface charging for small κ_i (~ 3) may be understood in the terms of availability of the high energy ion in the distribution, constituting higher ion current and compensates the electron collection current.

Considering the vibrant plasma atmosphere around Moon, it is of significance to relax the condition ($\tau = y = 1$) and analyse the effects of varying τ and y . The effect of varying τ on surface potential has been illustrated in Fig. 2a. The lunar surface potential monotonically increases with in-

creasing τ . Physically, this behaviour pertains to an increase in electron collection current with increasing T_{es} . Quantitatively, it may be understood in terms of the electron accretion current (Eq. (6c) and Eq. (7c)) dependence on κ and τ . The dependence of surface potential parameter x on parameter y has been shown in Fig. 2b. Noted, $y (= n_{es}/n_{is})$ refers to the physical situation where the number density of the electrons and ions in the plasma are different—this may hold in a case when the ions hold a higher charge state (other than the proton). The surface potential increases with an increase in the electron population associated with the accretion current. In the context of lunar regolith, the calculations corresponding to $y > 1$ may refer to the plasma environment in the wake and mini wakes—these structures form due to the solar wind plasma expansion downstream of the Moon and the obstructing object (like shadowed craters and highlands) on the lunar surface, respectively (Farrell et al. 2010). In the process of plasma expansion, due to smaller electron inertia, an electron-rich region appears in the leeward portion (Farrell et al. 2008). In the case of electron-rich plasmas, the electron inertia dominates in the surface charging process;

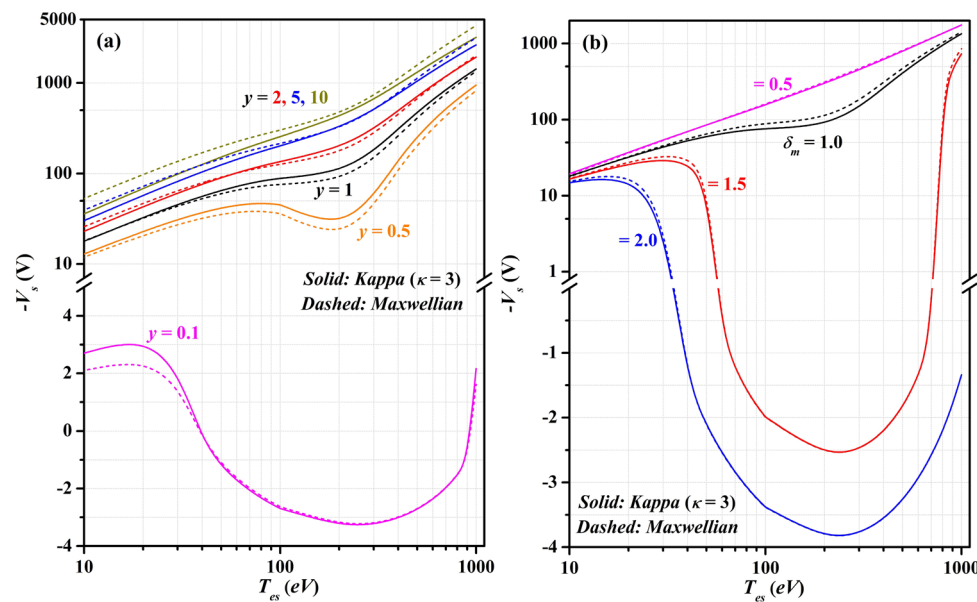


Fig. 3 Dependence of the surface potential V_s on the temperature of the plasma electrons T_{es} for dark region plasma, i.e., in the absence of the photoelectric emission. (a: left panel): refers to the variation of parameter y for $\delta_m = 1.0$ while the colour labels magenta, orange, black, red, blue and grey in the figure refers to the magnitude of the varying parameter $y = 0.1, 0.5, 1.0, 2.0, 5.0$ and 10.0 , respectively. (b: right

panel): refers to the variation of parameter δ_m for $y = 1.0$; the colour labels magenta, black, red and blue in the figure refers to the magnitude of the varying parameter $\delta_m = 0.5, 1.0, 1.5$ and 2.0 , respectively. The other parameters used in computations are $\tau = 1, z = 1/2$ and $\kappa = 3$. The solid and dashed lines refer to Kappa and Maxwellian velocity distribution of the plasma electrons/ions, respectively

the calculation suggests that the lunar surface may acquire significantly large negative potential for $y \gg 1$. Noticed, the Kappa distributed electrons predict significantly higher potential than that of Maxwellian electrons for $y \gg 1$; for instance, it is twice for $\kappa = 3$ and $y = 10$ (Fig. 2b). For $y < 1$, due to lower electron density, the contribution from the electron accretion current reduces with respect to the ion collection current, causing a reduced surface potential. Moreover, parametrically in reference to Eqs. (10)–(12), the variation in parameter y also infers the dependence of surface charging on relative sticking (z) for a $y = 1$; in general, for space plasmas $z < 1$ (Draine and Salpeter 1979; Weingartner and Draine 2001). Its dependence on κ is a consequence of the variation in electron collection current (Eqs. (6c) and (7c)) with the spectral index. These estimates (Fig. 1 and Fig. 2) do not include the effect of SEE from the lunar surface. However, considering the high energy electron population in the plasma around Moon, the significance of SEE in the lunar surface charging cannot be ruled out, particularly in the dark region plasma (i.e., in the absence of photoemission). Next, we examine the effect of SEE from the lunar surface in the case of dark plasma.

The SEE establishes a positive return current (like ion current) and effectively modifies the balance of charging currents over the lunar regolith. In the presence of SEE flux, a decrease in the negative potential is anticipated. Figure 3 represents a quantitative estimate of the lunar surface potential in dark region plasma as a function of the temperature

of the electrons for $\tau = 1$, and (Fig. 3a) different values of y for $\delta_m = 1$ and (Fig. 3b) different values of δ_m for $y = 1$; the computations refer to the sticking coefficient $\eta_i = 2\eta_e = 1$ and $z = 1/2$. The base axis T_{es} in the figure covers the complete measured range of the electron temperature in the local plasma atmosphere around Moon, i.e., terrestrial magnetosphere, solar wind, wake and SEP events (Halekas et al. 2008). The lunar surface potential evolves temporally until it attains a steady state; this time taken to reach steady state solution (i.e., τ_{ss}) may be obtained by solving Eq. (1) numerically and measuring the extent of ‘ t ’ when V_s becomes nearly independent of time. For instance, for the range of parameters used in deriving Fig. 3, i.e., $T_{es} = (10 \text{ eV} - 1 \text{ KeV})$ and $y = (0.1 - 10)$ and $n_{es} = 1 \text{ cm}^{-3}$, τ_{ss} varies in the range $\sim (30 \text{ s} - 400 \text{ s})$. This parameter τ_{ss} significantly depends on the plasma density, and our calculations show τ_{ss} decreases with increasing plasma density. Additionally, it may be noted that for the dark region plasmas, in the steady state, the parameter y is a significant parameter (and not n_{es}). In figure (Fig. 3), the steady state potential respectively varies in the range $\sim 2.0 \text{ V}$ to -4.0 kV . The effect of inclusion of SEE effect may immediately be seen by comparing the results of Fig. 2 and Fig. 3—in this case, the negative potential reduces with the inclusion of SEE flux. For instance, for $T_{es} = 100 \text{ eV}$ and $y = 1$, the surface acquires a potential $\sim -100 \text{ V}$ (Fig. 3) in the presence of SEE in comparison to $\sim 3T_{es} = -300 \text{ V}$. In the figure, an optimum in the steady state surface potential with respect to T_{es} is observed. This

nature can be understood in terms of SEE yield dependence on the energy of the impacting plasma electron (Eq. (8a)–(8c)), which takes an optimum with T_{es} . As depicted in Fig. 3a, the magnitude of the surface potential decreases with y and may take a positive value for $y = 0.1$. This can be explained in terms of a decrease in the electron plasma density, causing reduced electron accretion flux and given ion current. The surface acquires the higher negative potential for large y values—this is again a consequence of increasing electron flux for large n_{es} . For instance, at $T_{es} = 100$ eV and $\kappa = 3$, the surface acquires ~ -250 V for $y = 10$ than that of ~ -92 V for $y = 1$. For $y < 1$, the surface gets charged to a smaller potential; for example, the surface gains negative potential of ~ -44 V for $y = 0.5$, $T_{es} = 100$ eV and $\kappa = 3$. The effect of varying δ_m on the surface charging has been illustrated in Fig. 3b. The negative surface potential decreases in magnitude with increasing value of δ_m due to the increasing magnitude of the SEE flux. For the large values of SEE yield, the SEE return current may also bring the surface at a finite positive potential. However, the positive potential in dark region plasma over lunar regolith has not yet been observed and is contrary to the LP observations of the negatively charged lunar surface; in this perspective, a small value of SEE yield is more plausible (Halekas et al. 2009b). A marginal difference in the surface potential is noticed for Kappa and Maxwellian distributed electrons. This set of calculations correspond to the dark region plasma, i.e., in the absence of photoemission of the electrons from the lunar surface, is pertinent to the case of wake ($T_{es} \sim 50$ – 150 eV), SEP events in wake ($T_{es} \sim 50$ eV– 1 keV) and solar wind ($T_{es} \sim 5$ – 30 eV) plasma—for $\delta_m = 1$ and $y = 1$, the lunar surface attains the negative potential $\sim (85$ – 231 V), $\sim (85$ – 1750 V) and $\sim (10$ – 105 V), respectively (all values correspond to Fig. 3b). The calculated values are consistent and well within the range of the lunar potential calculated by Halekas et al. (2008) using LP plasma measurements.

Next, we include the effect of photoemission on the surface charging and discuss its implications to the sunlit locations on Moon. The photoemission flux is sensitive to the electronic properties of the regolith material, i.e., work function, photoelectric yield, and temperature of the emitting surface. In this case, the surface charging takes place under the mutual influence of photoelectron current and the ambient plasma collection. For the moderate plasma conditions, for instance, solar wind (\sim few eV electrons), the photoemission current in general dominates over the plasma accretion current and the surface may acquire finite positive potential. However, for the extreme plasma conditions, e.g., terrestrial magnetosphere/solar eruption (moderate density, keV electrons), the sunlit surface may attain a negative potential. A comparison of Kappa and Maxwellian based plasma has been significantly discussed in the earlier results (Figs. 1–3), for the sunlit regolith case, we present the results

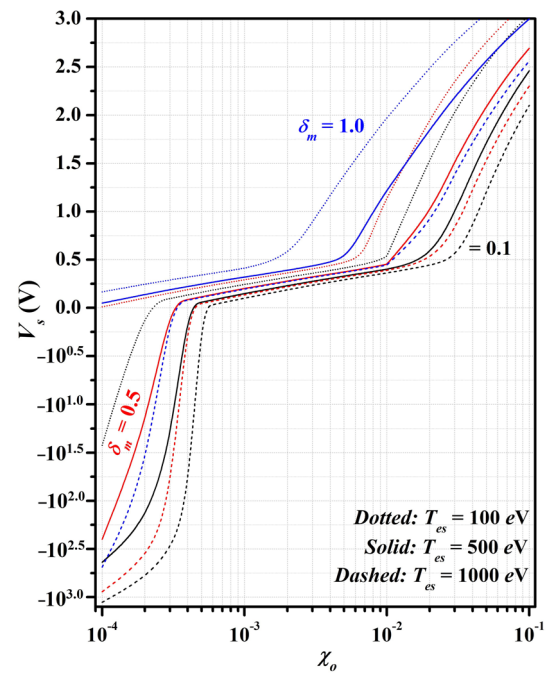


Fig. 4 Dependence of the surface potential V_s on the photoelectric efficiency (χ_o) for different values of the plasma temperature (T_{es}) and SEE yield (δ_m); the computations correspond to $z = 1/2$, $y = 1$, $\tau = 1$, $\phi = 6.0$ V, $n_{so} = 5$ cm $^{-3}$, $\theta = 70^\circ$ and $\kappa = 3$. The colour labels black, red and blue refer to the magnitude of the varying parameter $\delta_m = 0.1$, 0.5 and 1.0 , respectively. The dotted, solid and dashed lines refer to different values of T_{es} (eV) = 100 , 500 and 1000 , respectively, respectively. Noted that the y -axis is presented in decimal and logarithmic scales for $V_s > 0$ and $V_s < 0$, respectively

corresponding to Kappa energy distribution of the plasma population (Figs. 4–7). On account of the large photoelectron population in the case of the solar illumination, the surface potential achieves steady state much quicker than that for dark region plasma case; it takes few ms to few seconds, depending on plasma parameters. We numerically investigate and illustrate the effect of surface parameters on steady state charging of the sunlit lunar surface.

The dependence of lunar surface potential on the photoelectric yield (χ_o) in the steady state has been shown in Fig. 4, for different values of the plasma electron temperature (T_{es}) and SEE yield (δ_m); the computations correspond to $z = 1/2$, $y = 1$, $n_{so} = 5$ cm $^{-3}$, $\tau = 1$, $\phi = 6.0$ V, $\theta = 70^\circ$ and $\kappa = 3$. It should be noted that the y -axis is presented in decimal and logarithmic units for $V_s > 0$ and $V_s < 0$, respectively. Physically, the photoelectric yield (χ_o) is a measure of the fraction of the photon flux contributing to the photoelectron current from the lunar surface; the photoelectron current linearly varies with χ_o , as $\chi \propto \chi_o$. The surface potential increases with an increase in the photoelectric efficiency of the lunar regolith material. Its dependence may be understood in terms of the increase in the relative contribution of the photoemission current with respect to the given plasma population. The SEE current additionally

supports the photoemission current in neutralising the net plasma accretion current. The surface takes a negative potential (dominant) for the small values of χ_o while it acquires a finite positive potential for large χ_o values. For instance, consider the dashed black line curve corresponding to $\delta_m = 0.1$ and $T_{es} = 1000$ eV—the portion $\chi_o > 0.02$ corresponds to the large photoelectron population in comparison to the plasma density, while for shallow decaying portion ($0.0005 < \chi_o < 0.02$), the charge population and flux associated with the photoemission and plasma accretion are relatively comparable. For the region $\chi_o < 0.0005$, the electron plasma current significantly dominates over the photoemission current, and the lunar surface takes higher negative potential to balance the constituent current in the steady state. The surface potential increases and tends towards positive values with increasing value of the SEE yield and temperature of the plasma electron. The variation with SEE yield may correspond to an increasing contribution of SEE flux in charging equilibrium while the temperature dependence may be ascribed to an increase in the collection current of electrons. The figure indicates that the surface may acquire a large negative potential (~ 100 V), even in the sunlit locations for small χ_o , and large plasma parameters n_{so} and T_{es} ; such plasma parameters are consistent with terrestrial plasma sheet and extreme solar events. For instance, for $\chi_o = 0.0003$, $\delta_m = 0.1$ and $T_{es} = 1000$ eV, the surface may hold ~ -640 V while it takes ~ 1 V for $\chi_o = 0.05$. The inclusion of the SEE effect is noticed to increase surface potential.

The effect of varying regolith work function on the surface charging for different values of the plasma density (n_{so}) and SEE yield (δ_m) has been illustrated in Fig. 5; the computations correspond to $z = 1/2$, $y = 1$, $\tau = 1$, $\chi_o = 0.001$, $T_{es} = 100$ V, $\theta = 70^\circ$ and $\kappa = 3$. Physically, the work function represents the electric potential barrier for the electrons available for emission within the lattice. For given photon radiation, the photoelectron current reduces with an increase in the work function of the surface material, as depicted in Fig. 5. For low work function regolith, the surface may acquire a finite positive potential due to a significant contribution from the photoemission current—this is partially aided by the SEE current for finite δ_m . The change in the nature of the lunar surface charge for the large work function values is attributed to the condition when the electron accretion takes the lead over the net positive current i.e., SEE plus photoemission flux. The photoemission current reduces for large work function values, and the surface tends to acquire a high negative potential. For example, the lunar surface may acquire a negative potential of ~ -110 V for $\phi = 7.0$ V and $(n_{so}, T_{es}, \delta_m) = (5 \text{ cm}^{-3}, 100 \text{ eV}, 0.5)$ —this plasma environment is pertinent with the terrestrial plasma sheet parameter. The dependence of the surface potential on n_{es} may be attributed to an increase in the collection current of electrons

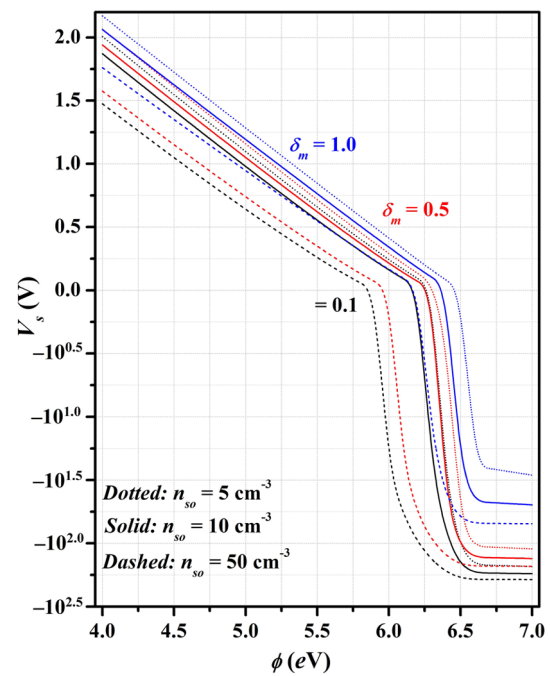


Fig. 5 Dependence of the surface potential V_s on the regolith work function (ϕ) for different values of SEE yield (δ_m) and plasma density (n_{so}); the computations correspond to $z = 1/2$, $y = 1$, $\tau = 1$, $T_{es} = 100$ eV, $\chi_o = 0.001$, $\theta = 70^\circ$ and $\kappa = 3$. The colour labels black, red and blue refer to the magnitude of the varying parameter $\delta_m = 0.1$, 0.5 and 1.0 , respectively. The dotted, solid and dashed lines refer to different values of n_{so} (cm^{-3}) = 5 , 10 and 50 , respectively. Noted that the y-axis is presented in decimal and logarithmic scales for $V_s > 0$ and $V_s < 0$, respectively

with increasing n_{es} ; the dependence has a similar trend as explained in the Fig. 4. The variation in the work function and the photoelectric yield on the lunar regolith may correspond to the neighbouring surfaces of different material compositions. This may lead to the differential charging of the neighbouring locations, resulting in a local electric field.

The dependence of the steady state surface potential on the temperature of ambient plasma has been shown in Fig. 6 for different values of the lunar latitude θ ; the computations correspond to $z = 1/2$, $y = 1$, $\tau = 1$, $\chi_o = 0.001$, $\phi = 6.0$ V, $\kappa = 3$, $\delta_m = (0.1, 0.5, 1.0)$ and $n_{es} = (5, 10, 50) \text{ cm}^{-3}$. The variation in the latitude (θ) affects the solar photon flux and the surface temperature, causing photoemission (Eq. (2)). The photon flux available for the photoelectric emission reduces with θ . Additionally, the decrease in the surface temperature with θ reduces the electron population density within the lattice, available for emission. The subsequent decrease in the photoemission current with increasing latitude θ reduces the surface potential. This effect with respect to electron temperature for varying δ_m and n_{es} are depicted in Fig. 6a and Fig. 6b, respectively. The lunar surface potential is noticed to decrease as one approach to the terminator region from the subsolar point ($\theta = 0$). The variation of lunar surface potential with the plasma temperature is primarily a

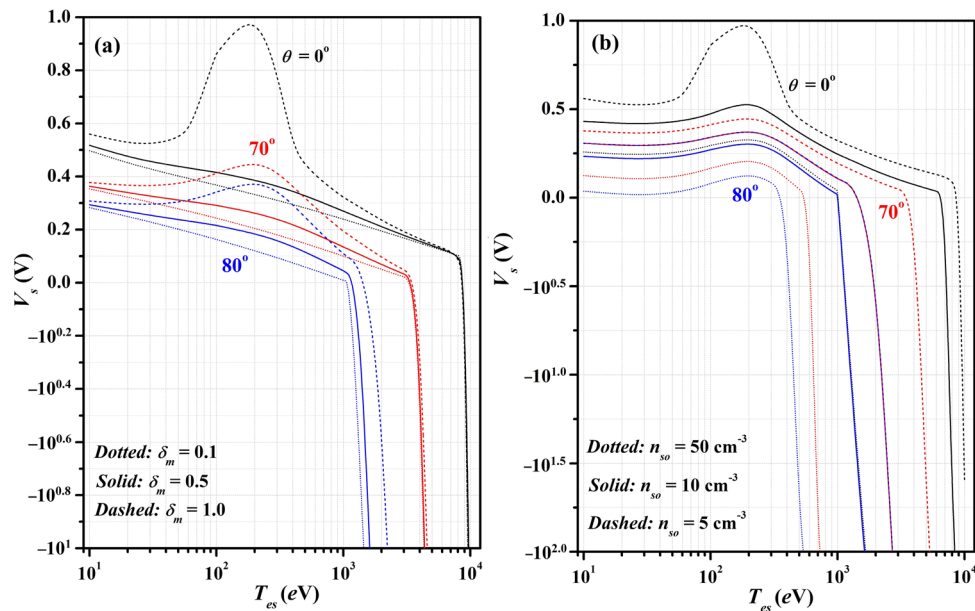


Fig. 6 Dependence of the surface potential V_s on the temperature of the plasma electrons T_{es} in the presence of simultaneous effects of Photoelectric and Secondary electron emission. **(a: left panel)**: refers to the variation of the SEE yield δ_m and lunar latitude (θ) for $n_{so} = 5 \text{ cm}^{-3}$; the colour labels black, red and blue refer to the magnitude of the varying parameter $\theta = 0, 70^\circ$ and 80° , respectively, while the dotted, solid and dashed lines refer to different values of the varying parameter $\delta_m = 0.1, 0.5$ and 1.0 , respectively. **(b: right panel)**: refers to the

variation of the variation of plasma density (n_{so}) and lunar latitude (θ) for $\delta_m = 1.0$; the colour labels black, red and blue refer to the magnitude of the varying parameter $\theta = 0, 70^\circ$ and 80° , respectively, while the dotted, solid and dashed lines refer to different values of the varying parameter $n_{so} (\text{cm}^{-3}) = 5, 10$ and 50 , respectively. The other parameters used in computations are $z = 1/2, y = 1, \tau = 1, \phi = 6.0 \text{ V}, \chi_o = 0.001$ and $\kappa = 3$. Noted that the y -axis is presented in decimal and logarithmic scales for $V_s > 0$ and $V_s < 0$, respectively

consequence of the increasing contribution of the electron accretion current with respect to that of the net emission (i.e., SEE plus photoemission) flux. The optimum magnitude of the surface potential with respect to the electron temperature may again be explained on the basis of SEE yield dependence of T_{es} . The variation in the lunar potential on δ_m and n_{es} show a trend similar to that explained in Fig. 5. The surface may carry significant negative potential near terminator for large temperature plasmas.

In Fig. 7a, we have shown the effect of variation of parameter y on the charging of the sunlit lunar regolith for different values of n_{is} and δ_m ; the computations correspond to $z = 1/2, \tau = 1, \phi = 6.0 \text{ V}, \theta = 70^\circ, T_{es} = 100 \text{ V}, \chi_o = 0.001$ and $\kappa = 3$. The parameter y in this calculation refers to the number density of the plasma electrons with respect to ion density in the ambient plasma. This effectively reduces (or enhance) the electron accretion current for $y < 1$ (or $y > 1$). The accreting plasma with $y > 1$ might lead the surface to a significant negative potential for large n_{es} values. For example, the lunar surface may acquire a significant negative potential of $\sim 110 \text{ V}$ for $(n_{es}, \delta_m, y) = (10 \text{ cm}^{-3}, 0.1, 10)$. As another variant, the dependence of the lunar surface potential on δ_m has been depicted in Fig. 7b for different values of y and T_{es} ; the computations correspond to $z = 1/2, \tau = 1, \phi = 6.0 \text{ V}, \theta = 70^\circ, n_{es} = 5 \text{ cm}^{-3}, \chi_o = 0.001$ and $\kappa = 3$. The dependence of the surface poten-

tial on the SEE yield may be understood in terms of increasing contribution of SEE flux with increasing δ_m in addition to a given photoemission flux. In this figure (Fig. 7b), the results corresponding to $\delta_m = 0$ and finite δ_m quantitatively show that the inclusion of SEE contributes to increasing the surface potential. These calculations suggest that the lunar surface may acquire significant negative potential, even in the sunlit locations; however, it requires large plasma density/temperature and small SEE yield values. For example, for $(T_{es}, \delta_m, y) = (1 \text{ keV}, 0.8, 10)$ the lunar surface corresponds to the negative potential of $\sim 1000 \text{ V}$. These results are particularly of interest for the partially shadowed or illuminated regions (e.g., electron-rich regions in crater mini wakes/sunlit highlands) where such plasma population may exist, and depending on the local plasma/surface/radiation parameters a huge potential contrast may exhibit in the neighbouring locations. Such differential charging may support the charge or particle transport locally.

8 Summary

The analysis brings out a physics insight of the photoelectric charging of the sunlit lunar regolith, exposed to the extreme ambient plasma corresponding to wake plasma, SEP

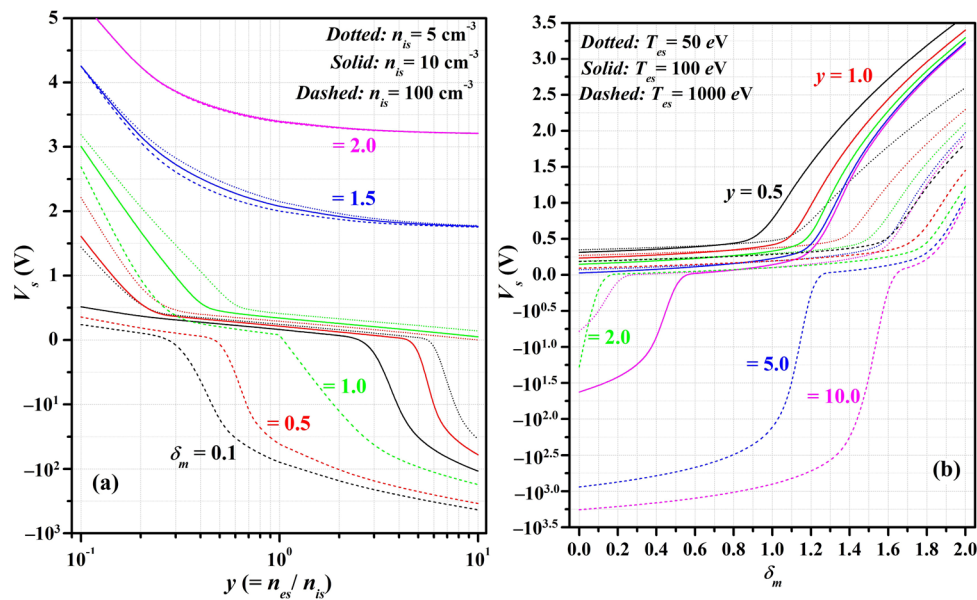


Fig. 7 (a, left panel): Dependence of the lunar surface potential V_s on the parameter y for different values of the SEE yield (δ_m) and plasma ion density (n_{is}); the computations correspond to $z = 1/2$, $\tau = 1$, $\phi = 6.0$ V, $\chi_o = 0.001$, $T_{es} = 100$ eV, $\theta = 70^\circ$ and $\kappa = 3$. The colour labels black, red, green, blue and magenta refer to the magnitude of the varying parameter $\delta_m = 0.1, 0.5, 1.0, 1.5$ and 2.0 , respectively, while the dotted, solid and dashed lines refer to different values of the varying parameter n_{is} (cm^{-3}) = 5, 10 and 100, respectively. (b, right panel): Dependence of the lunar surface potential V_s on the SEE yield (δ_m)

for different values of the parameter y and plasma electron temperature (T_{es}); the computations correspond to $z = 1/2$, $\tau = 1$, $\phi = 6.0$ V, $\chi_o = 0.001$, $n_{is} = 5$ cm^{-3} , $\theta = 70^\circ$ and $\kappa = 3$. The colour labels black, red, green, blue and magenta refer to the magnitude of the varying parameter $y = 0.5, 1.0, 2.0, 5.0$ and 10.0 , respectively, while the dotted, solid and dashed lines refer to different values of the varying parameter T_{es} (eV) = 50, 100 and 1000, respectively. Noted that the y -axis is presented in decimal and logarithmic scales for $V_s > 0$ and $V_s < 0$, respectively

events, and terrestrial magnetosphere. In order to establish the conceptual basis, the openness nature of the charge flux over lunar regolith has been included in writing the balance equation of the surface charging—the photoemission of electrons, secondary electron emission and accretion of the plasma electrons/ions are considered as dominant charging mechanisms. In evaluating the photoemission current, the full solar spectrum, including continuous radiation and dominant EUV Lyman- α photons along with adequate Fermi–Dirac (FD) distribution of the electron velocities within the lattice, has been consistently taken into account. As case studies, the ambient plasma is considered to exhibit the Kappa and Maxwellian distribution of their velocities. The temperature dependent SEE yield has consistently been accounted to evaluate the secondary electron emission current from the lunar regolith. The surface charging has been found a significant function of plasma parameters (number density/temperature) and material properties (viz. work function/photoefficiency).

In dark regions, i.e., in the absence of the photoelectric emission, the SEE mechanism contributes significantly in determining the equilibrium potential—the lunar surface may attain a negative potential, nearly of the order of the electron temperature in the plasma distribution for low values of the SEE yield. Furthermore, unlike the notion of positive potential over the sunlit location, a significant contrast

in the charging of the lunar surface, depending on surface and plasma parameters, is predicted, and it may differ by the orders of magnitude (Figs. 4–7). This is consistent with the observation of negative potential above the dayside lunar surface in the terrestrial plasma sheet (Halekas et al. 2009b). For instance, in reference to Fig. 7, the lunar surface may hold a negative potential of ~ 600 V for $\phi = 6.5$ V, while it acquires ~ 1.0 V in case $\phi = 5.0$ V. The results for the variation in regolith work function and photoefficiency reflects the possible disparity in the adjacent locations in terms of the material composition. A similar difference in the surface charging may occur for the topographical features, for instance, nearby highland and crater locations, where the rear side (i.e., opposite to sun-facing) is shadowed region—this may correspond to the smaller reach of solar photons, and the local plasma is a dominant source of charging. In such a case, the potential in the dark region (~ -100 V, Fig. 3) and adjacent illuminated (\sim few Volt, Fig. 4) portions of the Moon regolith may differ by orders of magnitude. In such extreme plasma conditions, the lunar regolith may lead to the differential charging, which might play a significant role in the transportation of local charge and fine charged dust in the lunar atmosphere. The present analytical model gives a feasible solution (and scaling) of the lunar surface charging and is of practical implications in conceptualising the test experiments in labs for future lunar studies.

Acknowledgement This work is supported by Department of Space, Government of India.

Publisher's Note Springer Nature remains neutral with regard to jurisdictional claims in published maps and institutional affiliations.

References

- Anderegg, M., Feuerbacher, B., Fitton, L.D., Wills, R.F.: In: LPSC, vol. 3, p. 266. (1972)
- Bauer, S.J.: *Physics of Planetary Ionosphere*. Springer, New York (1973)
- Chow, V.W., Mendis, D.A., Rosenberg, M.: *J. Geophys. Res.* **98**, 19065 (1993)
- Ciftja, O.: *Eur. J. Phys.* **32**, L55 (2011)
- Draine, B.T.: *Astrophys. J. Suppl. Ser.* **36**, 595 (1978)
- Draine, B.T., Salpeter, E.E.: *Astrophys. J.* **231**, 77 (1979)
- Farrell, W.M., Stubbs, T.J., Halekas, J.S., Delory, G.T., Collier, M.R., Vondrak, R.R., Lin, R.P.: *Geophys. Res. Lett.* **35**, L05105 (2008)
- Farrell, W.M., Stubbs, T.J., Halekas, J.S., Kilen, R.M., Delory, G.T., Collier, M.R., Vondrak, R.R.: *J. Geophys. Res.* **115**, E03004 (2010)
- Fowler, R.H.: *Statistical Mechanics: The Theory of the Properties of Matter in Equilibrium*. Cambridge University Press, London (1955)
- Goertz, C.K.: *Rev. Geophys.* **27**, 271 (1989)
- Goldstein, B.E.: *J. Geophys. Res.* **23**, 35 (1974)
- Gosling, J.T., Hildner, E., Asbridge, J.R., Bame, S.J., Feldman, W.C.: *J. Geophys. Res.* **82**, 5005 (1977)
- Grobman, W.D., Blank, J.L.: *J. Geophys. Res.* **74**, 3943 (1969)
- Halekas, J.S., Mitchell, D.L., Lin, R.P., Hood, L.L., Acuna, M.H., Binder, A.B.: *Geophys. Res. Lett.* **29**, 1435 (2002)
- Halekas, J.S., Delory, G.T., Lin, R.P., Stubbs, T.J., Farrell, W.M.: *J. Geophys. Res.* **113**, A09102 (2008)
- Halekas, J.S., Delory, G.T., Lin, R.P., Stubbs, T.J., Farrell, W.M.: *J. Geophys. Res.* **114**, A05110 (2009a)
- Halekas, J.S., Delory, G.T., Lin, R.P., Stubbs, T.J., Farrell, W.M.: *Planet. Space Sci.* **57**, 78 (2009b)
- Hinteregger, H.E., Hall, L.A., Schmidtke, G.: Solar XUV radiation and neutral particle distribution in July 1963 thermosphere. In: King-Hele, D.G. (ed.) *Space Research V*. North-Holland, Amsterdam (1965)
- Horanyi, M., Walch, B., Robertson, S., Alexander, D.: *J. Geophys. Res.* **103**, 8575 (1998)
- Johannsson, H.E.: *Handbook on Solar Wind: Effects, Dynamics, and Interactions*. Nova Science Publishers, New York (2009)
- Kimura, H.: *Mon. Not. R. Astron. Soc.* **459**, 2751 (2016)
- Livadiotis, G., Desai, M.I., Wilson, L.B.: *Astrophys. J.* **853**, 142 (2018)
- Mann, I., Kimura, H., Biesecker, D.A., Tsurutani, B.T., Grun, E., McKibben, R.B., Liou, J.-C., MacQueen, R.M., Mukai, T., Guhathakurta, M., Lamy, P.: *Space Sci. Rev.* **110**, 269 (2004)
- Mann, I., Pellinen-Wannberg, A., Murad, E., Popova, O., Meyer-Vernet, N., Rosenberg, M., Mukai, T., Czechowski, A., Mukai, S., Safrankova, J., Nemecek, Z.: *Space Sci. Rev.* **161**, 1 (2011)
- Meyer-Vernet, N.: *Astron. Astrophys.* **105**, 98 (1982)
- Mishra, S.K., Bhardwaj, A.: *Astrophys. J.* **884**, 05 (2019)
- Mishra, S.K., Misra, S.: *Phys. Plasmas* **21**, 073706 (2014)
- Mishra, S.K., Misra, S., Sodha, M.S.: *Eur. Phys. J. D* **67**, 210 (2013)
- Misra, S., Mishra, S.K.: *Mon. Not. R. Astron. Soc.* **432**, 2985 (2013)
- Misra, S., Mishra, S.K., Sodha, M.S.: *Phys. Plasmas* **20**, 013702 (2013)
- Nemecek, Z., Pavlu, J., Safrankova, J., Beranek, M., Richterova, I., Vaverka, J., Mann, I.: *Astrophys. J.* **738**, 14 (2011)
- Nitter, T., Havnes, O., Melandsø, F.: *J. Geophys. Res.* **103**, 6605 (1998)
- Pavlu, J., Richterova, I., Nemecek, Z., Safrankova, J., Cermak, I.: *Faraday Discuss.* **137**, 139 (2008)
- Pierrard, V., Maksimovic, M., Lemaire, J.: *Astrophys. Space Sci.* **277**, 195 (2001)
- Piquette, M., Horanyi, M.: *Icarus* **291**, 65 (2017)
- Pivi, M., King, F.K., Kirby, R.E., Raubenheimer, T.O., Stupakov, G., Le Pimpec, F.: *J. Appl. Phys.* **104**, 104904 (2008)
- Poppe, A., Horanyi, M.: *J. Geophys. Res.* **115**, A08106 (2010)
- Poppe, A., Halekas, J.S., Horanyi, M.: *Geophys. Res. Lett.* **38**, L02103 (2011)
- Poppe, A., Piquette, M., Likhanskii, A., Horanyi, M.: *Icarus* **221**, 135 (2012)
- Richterova, I., Nemecek, Z., Beranek, M., Safrankova, J., Pavlu, J.: *Astrophys. J.* **761**, 108 (2012)
- Richterova, I., Nemecek, Z., Pavlu, J., Safrankova, J., Vaverka, J.: *IEEE Trans. Plasma Sci.* **44**, 505 (2016)
- Seitz, F.: *Modern Theory of Solids*. McGraw-Hill, New York (1940)
- Sickafoose, A.A., Colwell, J.E., Horanyi, M., Robertson, S.: *J. Geophys. Res.* **106**, 8343 (2001)
- Sodha, M.S., Mishra, S.K.: *Phys. Plasmas* **21**, 093704 (2014)
- Sodha, M.S., Misra, S., Mishra, S.K.: *Phys. Plasmas* **16**, 123705 (2009)
- Sternglass, E.J.: *The Theory of Secondary Electron Emission*, Sci. Paper 1772. Westinghouse Res. Lab: Pittsburgh (1954)
- Sternovsky, Z., Chamberlin, P., Horanyi, M., Robertson, S., Wang, X.: *J. Geophys. Res.* **113**, A10104 (2008)
- Stubbs, T.J., Vondrak, R.R., Farrell, W.M., Collier, M.R.: *J. Astronaut.* **28**, 166 (2007a)
- Stubbs, T.J., Halekas, J.S., Farrell, W.M., Vondrak, R.R.: Lunar surface charging: a global perspective using lunar prospector data. In: Krueger, H., Graps, A.L. (eds.) *Dust in Planetary Systems*. ESA SP-643, p. 181 (2007b)
- Stubbs, T.J., Farrell, W.M., Halekas, J.S., Burchill, J.K., Collier, M.R., Zimmerman, M.I., Vondrak, R.R., Delory, G.T., Pfaff, R.F.: *Planet. Space Sci.* **90**, 10 (2014)
- Vaverka, J., Richterova, I., Pavlu, J., Safrankova, J., Nemecek, Z.: *Astrophys. J.* **825**, 133 (2016)
- Weingartner, J.C., Draine, B.T.: *Astrophys. J.* **134**, 263 (2001)
- Whipple, E.C.: *Rep. Prog. Phys.* **44**, 1197 (1981)
- Williams, J.P., Paige, D.A., Greenhagen, B.T., Sefton-Nash, E.: *Icarus* **283**, 300 (2017)
- Zaslavsky, A.: *J. Geophys. Res. Space Phys.* **120**, 855 (2015)